European Journal of Pharmaceutical Sciences 182 (2023) 106371

Contents lists available at ScienceDirect

European Journal of Pharmaceutical Sciences

journal homepage: www.elsevier.com/locate/ejps

Dissolvable microneedles for transdermal drug delivery showing skin penetration and modified drug release

Irina Iachina [e], André H. Eriksson [a], Malene Bertelsen [a], Karsten Petersson [b], Jörgen Jansson [b], Pernille Kemp [b], Karen M. Engell [c], Jonathan R. Brewer [e,*], Kim T. Nielsen [d,*]

[a] In Vivo Biology & Biomarkers, LEO Pharma A/S, Industriparken 55, Ballerup 2750, Denmark
[b] Explorative Formulation & Technologies, LEO Pharma A/S, Industriparken 55, Ballerup 2750, Denmark
[c] Small Molecule Early Pharmaceutical Development, LEO Pharma A/S, Industriparken 55, Ballerup 2750, Denmark
[d] Advanced Analytical and Structural Chemistry, LEO Pharma A/S, Industriparken 55, Ballerup 2750, Denmark
[e] Department of Biochemistry and Molecular Biology, University of Southern Denmark, Odense, Denmark

ARTICLE INFO

Keywords:
Dissolvable microneedle
Coherent anti-Stokes Raman scattering
Modified release
Calcipotriol
Betamethasone-17–21-dipropionate
Transdermal drug delivery
Human and porcine skin

ABSTRACT

Topical therapies for chronic skin diseases suffer from a low patient compliance due to the inconvenient treatment regimens of available products. Dissolvable microneedles (MN) with modified release offer an interesting possibility to increase the compliance by acting as a depot in the skin and thereby decreasing the dosing frequency. Furthermore, the bioavailability can be increased significantly by bypassing the barrier of the skin by the direct penetration of the MN into the skin. In this study the depot effect and skin penetration of an innovative dissolvable MN patch was assessed by insertion in *ex vivo* human skin and in vivo using minipigs. The MN patches are based on biodegradable polymers and the active pharmaceutical ingredients calcipotriol (Calci) and betamethasone-17–21-dipropionate (BDP) used to treat psoriasis. Using computed tomography (CT) and Coherent anti-Stokes Raman scattering (CARS) microscopy it was possible to visualize the skin penetration and follow the morphology of the MN as function of time in the skin. The depot effect was assessed by studying the modified *in vitro* release in an aqueous buffer and by comparing the drug release of a single application of a patch both *ex vivo* and *in vivo* to daily application of a marketed oleogel containing the same active pharmaceutical ingredients. The CT and CARS images showed efficient penetration of the MN patches into the upper dermis and a slow swelling process of the drug containing tip over a period of 8 days. Furthermore, CARS demonstrated that it can be used as a noninvasive technique with potential applicability in clinical settings. The *in vitro* release studies show a release of 54% over a time period of 30 days. The pharmacological relevance of MNs was confirmed in human skin explants and *in vivo* after single application and showed a similar response on calcipotriol and BDP mediated signaling events compared to daily application of the active oleogel. Altogether it was demonstrated that the MN can penetrate the skin and have the potential to provide a depot effect.

1. Introduction

Cutaneous drug delivery offers a promising alternative to conventional oral delivery or hypodermic injection. Compared to oral delivery cutaneous drug delivery bypasses the first-pass effect which encompasses both absorption and metabolism phenomena where the drug may be lost in the gastrointestinal tract and liver and can provide a localized treatment of skin pathologies with a better safety profile since the systemic exposure is minimized (Sabri et al., 2019). Cutaneous drug delivery systems are furthermore attractive from a patient compliance perspective compared to injection delivery (Cevc, 2004; Tanner and Marks, 2008; Wang et al., 2005), sonophoresis (Herwadkar et al., 2012), and lipid vesicle carriers (Cevc, 2004; Tanner and Marks, 2008), with the overall goal of creating more efficient intra and transdermal drug delivery. Furthermore, formulations with modified drug release offer the possibility of reduced dosing and thereby improved compliance.

MNs are a promising technology that can overcome the limitations of skin permeability and help with patient compliance by offering modified release. The arrays consist of small needles, usually in the size range of 100 to 1000 μm; which means they penetrate the SC and do so without

* Corresponding authors.
E-mail addresses: brewer@memphys.sdu.dk (J.R. Brewer), ktidk@leo-pharma.com (K.T. Nielsen).

https://doi.org/10.1016/j.ejps.2023.106371
Received 6 September 2022; Received in revised form 12 December 2022; Accepted 2 January 2023
Available online 5 January 2023

stimulating the dermal nerves making it a pain-free procedure (Bal et al., 2008; Haq et al., 2009; Kaushik et al., 2001). There are several different applications of MNs. One type of application is using an array of solid needles; prepared using silicone, metal (Cormier et al., 2004) or polymers(Sullivan et al., 2010), which are applied to the skin and subsequently removed. A drug formulation can then be added to the microchannels created by the needles and the drug then passively diffuses into the skin (Quinn et al., 2014). Another type of MNs uses soluble/dissolving needles containing the active ingredient. These needles are usually made of a soluble matrix such as sugars; carbohydrates or synthetic polymers loaded with the drug (Sullivan et al., 2008). When these needles are inserted into the skin the matrices dissolve, releasing the drug molecule. Dissolving needles have been shown to deliver a range of different substances and, by altering the matrix, different release profiles can be obtained (Ito et al., 2012; Jakka et al., 2022; Liu et al., 2012) (Donnelly et al., 2014; Gomaa et al., 2012; Matsuo et al., 2012a, 2012b; Naito et al., 2012).

In this study, we evaluate an innovative MN (Petersson et al., 2016), loaded with the drugs betamethasone-17,21-dipropionate and calcipotriol (see the structures in supplementary Fig. S1) for treatment of psoriasis (Lind et al., 2016). The MNs consist of an adhesive patch with an array of microneedles combining the ability of the microneedles to penetrate the SC with the ability of leaving a depot in the skin, facilitating both high intradermal drug delivery and improved patient compliance due to the lower number of treatments needed. The needles are two-component needles composed of a fast-dissolving base which dissolves quickly after penetrating the skin by the humidity of the skin leaving the needle's tip loaded with the drugs in the skin. The tip is designed to act as a depot slowly releasing the drug molecules into the dermal microcirculation.

Typical methods to characterize the penetration and/or drug delivery of MN-based drug delivery systems are computed tomography (CT) scanning (Loizidou et al., 2016), optical coherence tomography (OCT) (Donnelly et al., 2010), laser scanning confocal microscopy (LSM) (Sullivan et al., 2008), ultrasound scanning (El Gammal et al., 1999), matrix-assisted laser desorption/ionization mass spectrometry imaging (MALDI-MSI) (Nguyen et al., 2018) and recently Raman based techniques such as confocal Raman, Coherent anti-Stokes Raman scattering (CARS) and stimulated Raman scattering (SRS) (Evans et al., 2005; Evans and Xie, 2008; Zumbusch et al., 1999). While CT scanning, OCT, ultrasound scanning, and LSM can non-invasively visualize the needles in the skin, they lack the chemical sensitivity to visualize drug release. Furthermore, due to the limited working area of OCT and ultrasound scanning - usually <0.5 cm^2 – only small or parts of patches can be tracked over time using these techniques. Confocal Raman and MALDI-MSI have the ability to visualize the drug release in the skin, however, the techniques are quite invasive typically requiring prepared tissue slices. Recently CARS and SRS have been shown to be interesting techniques that can facilitate non-invasive, label-free chemically specific imaging in skin samples (Thorsted et al., 2019). CARS is an optical microscopy technique that allows imaging under near-physiological conditions, but with CARS no labeling is needed as it enables imaging of specific chemical bonds (Denk et al., 1990) (Saar et al., 2010). As CARS is a multi-photon technique optical sectioning is also possible with a high z-resolution enabling investigation of the complete penetration of the needles in the skin.

The assessment of intradermal drug concentrations after the application of MNs is technically challenging due to drug containing tips residing in the skin. This makes the differentiation between drugs residing in the tip and drugs released from the tip challenging. Several approaches have been developed to address these challenges and quantifying intradermal free drug concentrations, such as quantitative imaging, microdialysis and microperfusion (Baumann et al., 2019; Bodenlenz et al., 2016; Bonnel et al., 2018; Handler et al., 2021).

An alternative approach is to assess bioavailability through the quantification of pharmacodynamic responses induced by released drug in the subjects. Calcipotriol is an agonist of the Vitamin D3 receptor and target engagement can be assessed by quantifying downstream signaling events such as CD14 gene expression (Schauber et al., 2007). Similarly, steroid receptor target engagement by betamethasone-17, 21-dipropionate leads to gene expression of FKBP5 (Sevilla et al., 2010). An orthogonal method of drug release assessment is the quantification of drug metabolites. Betamethasone-17,21-dipropionate is metabolized to betamethasone-17-propionate by skin esterases and thus the presence of betamethasone-17-propionate is indicative of the release of the parent compound (Khattak et al., 2012).

The microneedle patches are intended to reduce the frequency of drug application and as such the assessment of in situ drug release is dependent on a biological system viable and intact for at least one week. The advancement of *ex vivo* human skin culture has brought forward the possibility of studying drug disposition and biomarkers in a human system. The NativeSkin® model is such a model, offering the possibility of studying repeated topical application on viable human skin for more than one week (Norsgaard et al., 2014). A potential drawback of using *in vitro* models is the lack of active drug clearance mechanisms in the form of blood flow and lymphatic drainage. Thus, complementary studies performed on for example Gottingen minipigs can be used to give valuable complementary data on the release in the *in vivo* setting.

In this study, both CARS microscopy and CT scanning were used for the investigation of needle penetration in human skin and porcine skin respectively. CARS and CT scanning were used to temporally study the 3-dimensional shape of the needles in excised human and porcine skin over a period of up to 8 days. Thus, facilitating characterization of the penetration of the needles and the dynamics of the depot tip left in the skin over time. The MNs were characterized in vitro using scanning electron microscopy (SEM), optical microscopy, and CARS.

To investigate the release and bioavailability of the MN patches *in vitro* experiments were carried out using SPF minipigs and in *ex vivo* human skin culture using the NativeSkin® model. Biopsies from the minipigs and NativeSkin® model were analyzed with RNA sequencing and LC/MS-MS for relevant biomarkers and metabolites.

2. Materials and methods

2.1. Human skin for imaging

The full thickness human skin samples used were obtained from healthy subject following abdominoplasty operations at Odense University Hospital. The samples were kept at –80 °C before use. For CARS microscopy 1.5 × 1.5 cm^2 large samples of skin were prepared. The samples were placed with the dermis side down on filter paper hydrated with PBS (Phosphate-buffered saline) buffer. MNs were manually applied to the skin using gentle pressure. After one hour the patch from the MN was removed and the samples were placed in an Ibidi glass bottom microscope dish with the needles and SC side downwards towards the glass. The samples were kept hydrated using PBS wetted filter paper placed on the dermis side of the sample. For prolonged imaging, the samples were kept at 32 °C.

All skin material was sampled in accordance with Danish national legislation and the declaration of Helsinki. The approval of use was authorized by the Regional Research Ethics Committee of Southern Denmark. The identities of the donors were anonymized and tissue was donated following informed written consent.

2.2. Microneedle array construction

Fig. 1 is a graphic illustration of a microneedle patch before insertion into the skin. Each 500 μm long needle consists of a fast dissolving backing layer, polyvinylpyrrolidone, PVP, (Kollidon® 17 PF from BASF ChemTrade GmBH, Germany) and a slowly degrading tip layer, poly (lactic-co-glycolic acid), PLGA, (Resomer® RG502 from Evonik Nutrition & Care GmBH, Germany) in which the drugs are molecularly

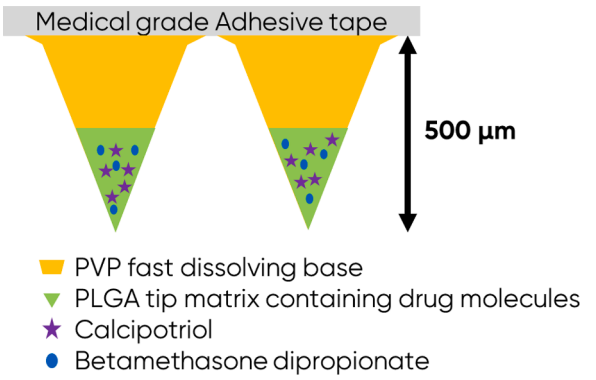

Fig. 1. Graphic illustration of the construction of the microneedle patch.

dispersed. The needle patches were made by casting the needles in a custom-made mold from RauMedic, Münchberg, Germany). For further details about manufacturing refer to (Petersson et al., 2016).

After insertion into the skin the PVP layer dissolves and the medical grade adhesive tape can thus be removed after two hours. The tip portion of the microneedles is designed to stay in the viable layers of the skin and to release the drug slowly over time. Each microneedle patch is 1.4 cm^2 and contains 49 needles in a 7 × 7 array. Each patch contains 1 µg calcipotriol and 12.6 µg betamethasone dipropionate. The marketed product Daivobet® gel was used as reference and is an oleogel that contains 50 µg/g calcipotriol and 0.643 mg/g betamethasone dipropionate, hence the same ratio between the two actives as in the microneedles.

2.3. Application of Microneedle arrays to skin

Microneedle arrays were applied to skin samples by firmly pressing the patch onto the skin samples. Samples were left for 60 min where after the adhesive tape was carefully removed and further investigation of the samples could be performed.

2.4. Electron microscopy (SEM)

SEM images were taken with a FEI Nova NanoSem equipped with a SensoFar PluNeox microscope with a voltage of 10 kV. To ensure high quality images of the polymer based MNs a thin gold coating was applied to the patch.

2.5. CT scanning

Prior to insertion in skin the MNs were sputter-coated with an approximate 100 nm thick layer of gold to provide sufficient contrast in the CT images. The coating was done using a Leica EM SD 500 coater using 40 mA for approximate two minutes. The CT images of microneedles inserted into porcine flank skin, were obtained using a Panalytical Empyrean multi-pose diffractometer equipped with a CT stage and a Cu x-ray tube with a point-shaped window. The source voltage and current of the x-ray tube were set to 20 KV and 20 mA respectively and scans were collected at 360° with an exposure time of 440 ms and rotation steps of 0.1 deg. A 0.1 mm Al filter and collimator of 7 mm were placed between the x-ray tube and the sample. Standard mode reconstruction was performed using VGStudio MAX version 3.0

2.6. Release studies

The *in vitro* release of betamethasone dipropionate (BDP) from the dissolvable patch was tested at 37°C in 10% w/w hydroxypropyl-β-cyclodextrine, pH 6.6. The microneedle patch contains 12.6 µg BDP/patch and 0.980 µg calcipotriol/ patch. The *in vitro* release was measured based on BDP. The pH of the release media was selected so BDP should be fairly hydrolytically stable, i.e., less than 10% degradation in 4 weeks, and so pH is close to a physiologically relevant pH. Hydroxypropyl-β-cyclodextrins were added to the release media to ensure sink condition since the aqueous solubility of BDP is only 1 µg/ml. Addition of 10% w/w of hydroxypropyl-β-cyclodextrins increases the solubility to 0.2 mg/ml.

A 20 ml screw-cap vial with 4.0 ml release media was placed in a Gerhardt Termoshake heating cupboard at 37°C for approximately 30 min to equilibrate.

One microneedle patch was added to each container with release media and gently shaken in the Gerhardt Termoshake heating cupboard at 37°C with a rotation speed of 100 RPM.

200 µl sample was removed after 0.5, 2, 4 and 6 h and then daily every workday for 30 days. The 200 µl sample is replaced with 200 µl fresh release medium that had been pre-heated to 37°C. The samples were analysed for content of BDP using reversed phase HPLC with UV detection at 240 nm. The separation was performed using a Thermo Scientific Accucore C18 (150 × 2.1 mm, 2.6 µm) column operated at 25 °C, and a gradient from 40% to 90% acetonitrile over 13 min. The pH was kept at 6.4 using a 0.01 M diammoniumphosphate pH 6.4 buffer as the aqueous part of the mobile phases. The injection volume was 50 µL and the flow rate was 0.35 mL/min.

2.7. Excitation & emission spectra

Single photon fluorescence emission spectra were measured on a Leica SP8 (Manheim; Germany). The excitation laser used was a pulsed white light laser. The system was equipped with a hybrid detector and used gated detection. Images were collected using galvo scanners. A 20X dry objective (NA=0.75) lens was used.

2.8. CARS

CARS images of needles were imaged using a Leica SP8 (Manheim; Germany). The pump and stokes beams were generated by a picosecond laser (pico Emerald, APE, Berlin , Germany) at 869 nm and 1064 nm respectably. This corresponds to a vibrational wavenumber of 1750 cm^{-1}. Auto-fluorescence and second harmonic generation were excited by the pump laser and imaged simultaneously. The system was equipped with 2 non-descanned PMT detectors in the forward and 2 in the epi-direction. For CARS images a band pass filter (661 nm ± 5.5) was placed in front of the CARS detector and for auto-fluorescent, a band pass filter (475 nm ± 100) was placed in front of the auto-fluorescence detector. Images were collected using the galvo scanners. A 40X IRAPO water objective (NA=1.1) lens was used in all the measurements.

2.9. Ex vivo human skin studies

Ex vivo human skin from abdominoplasty was obtained through Genoskin (Toulouse, FR). Specifically, 18 NativeSkin® XL models with an available surface area of 2.54 cm^2 were obtained from each of three donors giving a total of 54 skin models. The donors were females aged 49 – 64 years. The skin models were kept in culture according to the supplier's protocol. For each donor, the skin models were treated in duplicates for active microneedles and singlets for other conditions. With skin from three donors used, a total of three or six determinations per treatment was performed. Microneedle patches were applied on Day 0. Daivobet® Gel, 15 µl gel (equivalent to the drug load in one MA patch) was applied on Day 0, 1, 3, 4 and 5.

After 1, 4 and 6 days the skin models were sampled for histological evaluation, qPCR analyses of biomarkers and LC/MS-MS analyses of betamethasone dipropionate and metabolite.

2.10. In vivo study

The study was performed at CitoxLab (Lille Skensved, DK). The study was performed in 3 female Göttingen SPF minipigs originating from Ellegaard Göttingen Minipigs A/S, Denmark. The animals were approximately 6 months old with a body weight of 14.3–14.7 kg at the start of the study. The pigs were treated on 2 × 2 cm test fields along the flank. Daivobet® Gel, 15 μl gel was applied on Day 0 or Day 3 or daily on Day 0 – 4. A placebo gel was applied daily on Day 0–4, MN patches containing calcipotriol and betamethasone dipropionate were applied on Day 0 or Day 2 and placebo microneedles were applied on Day 2. The animals were euthanized on Day 5 immediately followed by skin biopsy sampling. From all test fields one 4 mm biopsy was placed in RNA*later* (ThermoFisher,) for subsequent gene analysis and one 8 mm biopsy was flash frozen for subsequent analysis by LC/MS-MS.

Animal experimental procedures as well as animal housing and husbandry were in compliance with Danish legislation and the EU Directive. The animal experiment permit was approved and granted by the Danish authorities for animal experimentation.

2.11. qPCR analyses

Skin biopsies were homogenized on the Precellys 24 apparatus and RNA extracted using the mirVana miRNA isolation extraction kit (ThermoFisher). Following cDNA synthesis, relative gene expression levels of CD14 (PD marker for calcitriol) and FKBP5 (PD marker for BDP) were determined by real-time quantitative PCR (qPCR) using Taqman® assay probe sets. Human samples: CD14 (Hs02621496_s1), FKBP5 (Hs01561006_m1). A panel of four reference genes (PPIA (Hs99999904_m1), RPLP0 (Hs99999902_m1), GAPDH (Hs99999905_m1), ACTB (Hs01060665_g1)) was used for qPCR data normalization. Minipig samples: CD14 (Ss03818718_s1), FKBP5 (AIY90KL) TBP (AI89LY7) and B2M (Ss03391154_m1) were used for qPCR data normalization.

2.12. Metabolite analyses

The skin biopsies were allowed to reach ambient temperature for approximately 1 hour. 10.0 μL working solution of the internal standard ALIS (1.00 μg/mL BDP-d10/B17P-d5, 0.500 μg/mL Calci-d4 and 0.25 μg/mL MC1080-d4 in methanol), 2 mL diethylether and 1.0 mL Cyclohexane were added. The samples were placed in an overhead shaker for 15 min. The diethylether/cyclohexane phase was transferred into a conical glass tube and the samples were evaporated to dryness at 40 °C under a gentle stream of nitrogen for approximately 30 min. The residue was dissolved in 50 μL methanol, vortexed and diluted with 50 μL HPLC-water. The samples were vortexed once again, centrifuged (5 min at 4000 rpm) and transferred into DW96 well plates. The plates were centrifuged for 2 min at 4000 rpm. An aliquot was injected into the LC-MS/MS system.

The remaining extracted biopsies were retained for control reasons and stored at –20 °C ± 5 °C.Concentrations of B-17-P metabolite were assessed using liquid chromatography-mass spectrometry to determine distributions of the drug molecules.

The LC-MS/MS system consisted of a Sciex API 5000 triple quadrupole mass spectrometer (Framingham, MA, USA) equipped with a Shimadzu HPLC pump (LC-20AD, Kyoto, Japan) using a CTC-analytics autosampler (HTC-PAL). The analytes were separated by a Phenomenex Synergi MaxRP (100 × 2.0 mm, 2.5 μm) column operated at 20 °C and mobile phases consisting of 800 mL methanol + 200 mL acetate buffer (1 mM Lithium acetate buffer + 2 mM Ammonium acetate buffer). The chromatrography was run isocratic with a run time of 12 min. The injection volume was 10 μL and the flow rate was 0.2 mL/min. The mass spectrometer was operated in positive ion mode with electrospray ionization and MRM scan. The B-17-P metabolite was quantified using the transition m/z 449.3 → 355.1 (Li adduct).

3. Results

3.1. Needle characterization

MN patches were made, as described in the methods section, and characterized using SEM and CARS microscopy. Fig. 2A shows a schematic representation of the needle used in this study before and after the PVP base has been dissolved during the hydration process in the skin, and Fig. 2B shows an image of a part of the patch with 49 needles.

Fig. 2C is a SEM image of a needle showing the characteristic pyramid shape of the needles. The needles were typically 200 μm wide at the base and 500 μm high.

To further characterize the needles fluorescence emission spectra and confocal images of needles containing no active compounds (placebo) and needles containing the active compound were collected (see Fig. 3). From Fig. 3A it can be seen that the active and the placebo needles show green auto fluorescence. The base and tip of the needle can clearly be discerned. When excited at 470 nm the tips of both the active and placebo needles have maximum emission at 522 nm. And the base of both the active and placebo needles has maximum emission at 480 nm. No substantial difference in the spectra between the placebo and active needles was seen.

CARS images and spectra of the placebo and active needles were acquired (see Fig. 4). The tip and the base could clearly be differentiated, however, no major difference between the active and placebo needles was seen. This implies that CARS could not be used to study the distribution of the drug molecule in the needles. The CARS spectra (Fig. 4A) showed 3 main peaks at 1750 cm^{-1}; 1639 cm^{-1} and 1424 cm^{-1}. The peak at 1750 cm^{-1} was only seen in the tip and not in the base. Imaging was mainly performed at 1750 cm^{-1}. For comparison a CARS spectrum of the human epidermis can be seen in Fig. S2.

Based on the SEM, LSM and CARS imaging of the needles it could be seen that the microneedles in the arrays clearly consist of a separate base and tip material. Furthermore, the tip polymer adheres to the side of the mold during the casting/ drying process forming a characteristic shape as depicted in Fig. 2.

The *in vitro* release of the drug molecules from the needles was done exclusive on betamethasone dipropionate (BDP) since the concentration of calciprotriol is so low due to the high potency that it is not possible to follow using traditional UV detection. The *in vitro* release of BDP was determined for six individual microneedle patches at 37°C in 10% w/w hydroxypropyl-β-cyclodextrins, pH 6.6. The release of BDP was a "burst" release of 40% of dose after 0.5 hour, followed by a slow release over the next 30 days. Hence, the release of BDP was 52% and 54% of dose after 21 and 30 days respectively. The data is shown graphically in Fig. 5. The "burst" release is probably due to the release of drugs on and close to the surface, which more and less is controlled by the dissolution rate of the drug molecules in the media. The slow release of the remaining 60% of the dose originate from the drugs deeper inside the needle and is controlled by the swelling, diffusion through the polymer matrix, water-mediated transport processes and degradation of the PLGA polymer by hydrolysis and erosion. However, there is a general lack in the understanding of the correlation between the release in the *in vitro* settings to *in vivo*. Investigation of the release of triamcinolone acetonide from PLGA microspheres indicate that the release *in vivo* is increased compared to *in vitro* settings. (Doty et al., 2017)

No sign of degradation of BDP was seen throughout the course of the study, i.e. none of the degradation products were detected.

3.2. Needles in human and porcine flank skin

To document the penetration of the needles into the skin both CT scanning and CARS microscopy were applied. MN arrays were applied to the skin samples as described in the material and methods section and imaging was performed after the adhesive tape was removed. In the case of the CT scans porcine skin was used. As described in the materials and

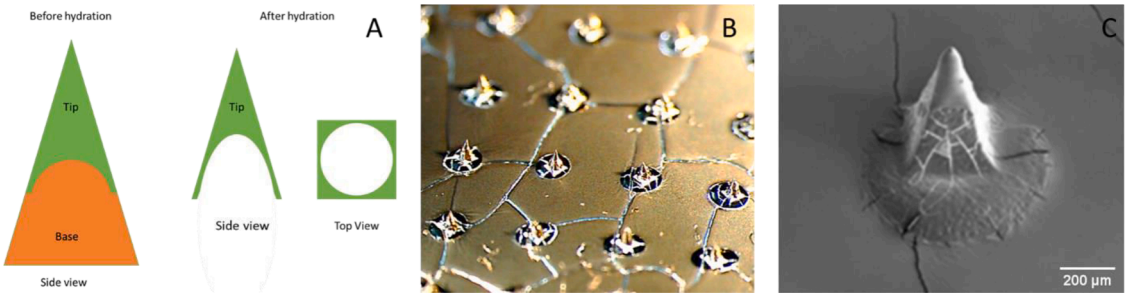

Fig. 2. (A) Schematic representation of the needle in this study, before and after hydration, as shown by CARS and multiphoton excitation microscopy. To the left shows the needle from the side, which is divided into a base and a tip, the latter which contains the active substance. To the right is the top view of the needle. (B) Image showing a part of the patch with 49 needles. (C) SEM image of a characteristic microneedle.

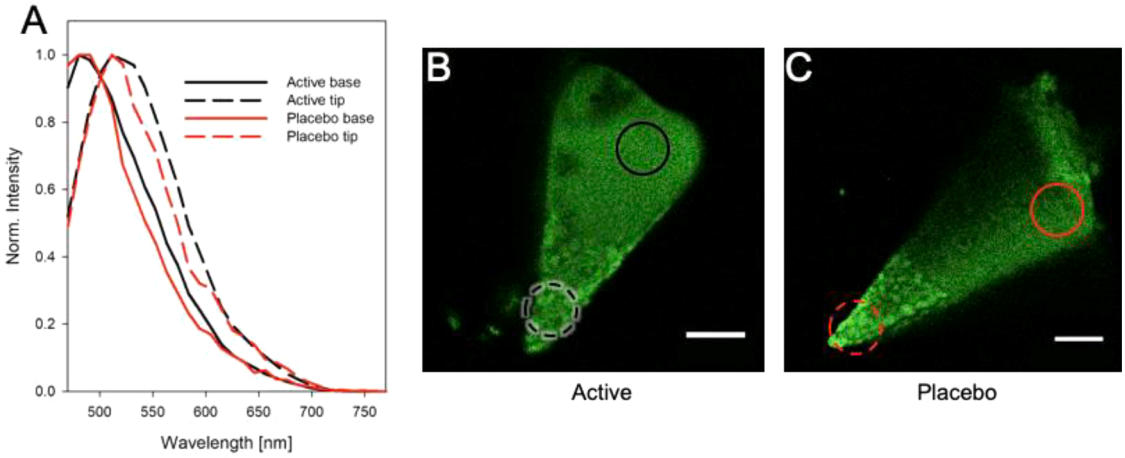

Fig. 3. Emission spectra of a placebo and active needle. (A) Emission spectrum with the normalized intensity as function of wavelength [nm] for the tip of a placebo needle (dashed red); the base of a placebo needle (solid red); the tip of an active needle (dashed black) and the base of an active needle (solid black). (B) A fluorescence image of an active needle showing where the emission was measured for the tip of the needle (dashed circle) and the base of the needle (solid circle). Scalebar is 100 µm. (C) A fluorescence image of a placebo needle showing where the emission was measured for the tip of the needle (dashed circle) and the base of the needle (solid circle). Scalebar is 100 µm.

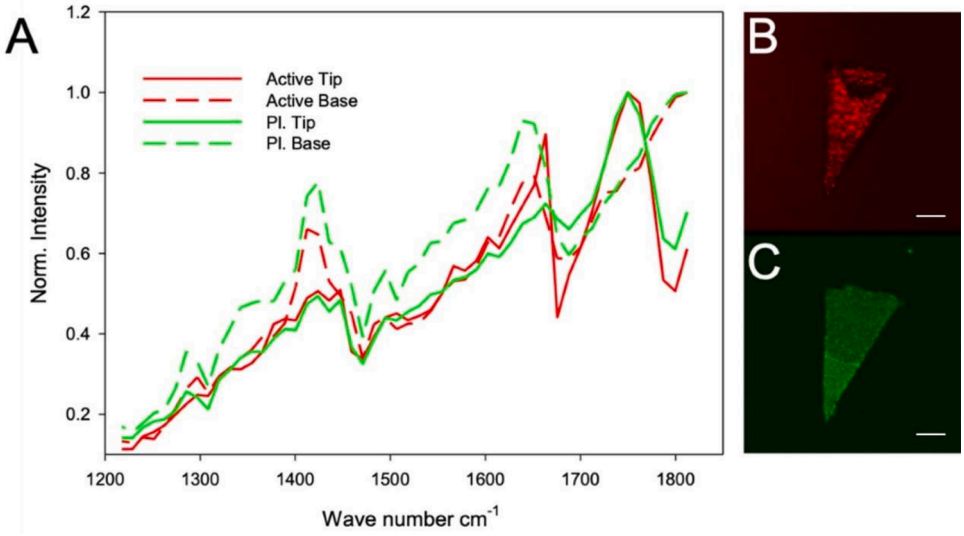

Fig. 4. (A) CARS spectrum with the normalized intensity as function of wave number [cm^{-1}] for the tip of a placebo needle (solid green); the base of a placebo needle (dashed green); the tip of an active needle (solid red) and the base of an active needle (dashed green). (B) A CARS image of an active needle imaged at 1770 cm^{-1}. (C) Auto-fluorescent signal of the same needle as in B. Scale bar is 100 µm.

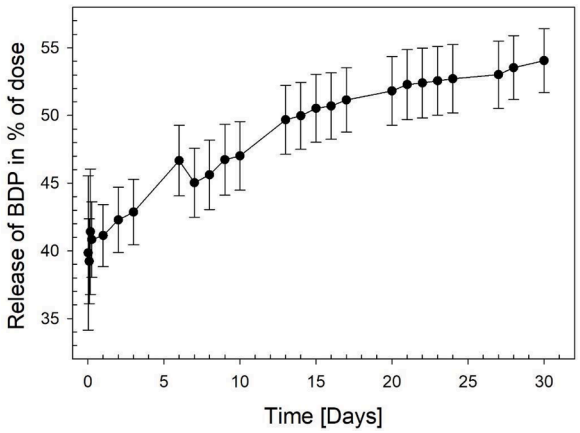

Fig. 5. *In vitro* release of BDP as% of dose as a function of time in days ($n = 6$). Error bars show standard deviation.

methods section the arrays were coated with gold prior to CT scanning to increase contrast. Fig. 6 shows horizontal sections at different depths in the skin. The needles could be seen down to about 200 μm depth in the skin showing a clear penetration of the SC.

Using a combination of CARS and multiphoton excited fluorescence microscopy it was possible to image penetration of placebo MNs into excised human skin. An overview image of the whole patch (1.4 cm^2) could be taken at multiple depths. Fig. 7 shows an overview image of the needles taken at the surface (Fig. 7A) and a higher magnification image showing how a single needle penetrates the skin (Fig. 7B). The red color shows the 2850 cm^{-1} CARS signal which is chosen to show the lipids in the skin, while the green channel shows autofluorescence and second harmonic generation (SHG) from collagen. The presence of the SHG from the collagen together with the signal from the needles clearly demonstrates that the needles have penetrated the SC and epidermis.

To demonstrate the microneedle penetration; stacks of images were collected at increasing depths (z stacks). This was performed for both placebo and active needles.

Fig. 7B shows the structure of the needles with the base material as the red color, which is clearly melted on top of the skin and the active tip as the bright green. The tips of the needles were seen to penetrate 250 μm below the surface of the skin and below the collagen present in the dermis. This demonstrates that the microneedle has successfully penetrated the epidermis and into dermis. This is in fully accordance with reported in the literature, where it is stated that polymer based dissolvable MNs penetrate between 1/2 and 2/3 of their length.(Ripolin et al., 2017)

To study the change in morphology of the microneedles over time four needles were followed over a time period of 8 days. Z stacks of the needles were recorded at 1 h; 2hours; 4 h; 24 h; 2 days; 4 days; 7 days and 8 days. The montage in Fig. 8 depicts a needle visualized at different depths at the time points: 1 hour; 4 h; 24 h and 8 days. The needle is seen to still be present after 8 days. However, some gradual deformation and shortening of the needles is seen and also penetration of the base material down towards the needle tip.

3D renderings of the needles after 1 hour and 8 days can be seen in Fig. 9, where again the overall structure of the needles can be seen with the base material shown as red and the active tip as a green edge surrounding the tip. It can be seen that the base material at 1 hour does not reach the bottom of the needle. After 8 days the needle tip is slightly deformed, and the base material now fills out the needle tip

The release from the needles was studied *ex vivo* using a human NativeSkin® model and *in vivo* using Göttingen minipigs. The release from the microneedle was compared to the daily application of a comparator gel (Daivobet® Gel). The results shown in Fig. 10 demonstrate prolonged Vitamin D and steroid mediated target engagement and elevated BDP metabolite levels, on par with the once daily application of the comparator Daivobet® Gel both in the NativeSkin® model and in the Göttingen minipigs.

The *ex vivo* studies show that for CD14, FKBP5 and B-17-P metabolite the MNs applied only on day 0 perform equal to the gel applied daily. Specifically, for CD14 for both the patch and gel it can be seen that the

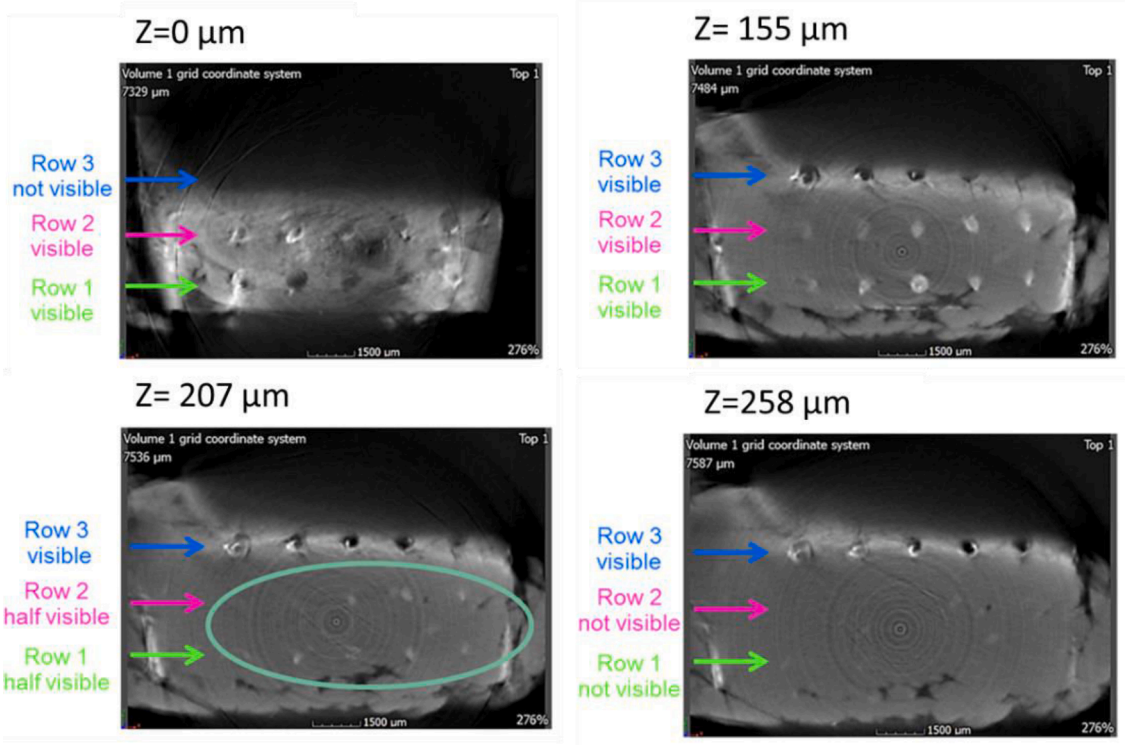

Fig. 6. CT scans of MN in porcine skin. The images show horizontal slices at increasing depths in the skin. The depth into the skin is shown above each image.

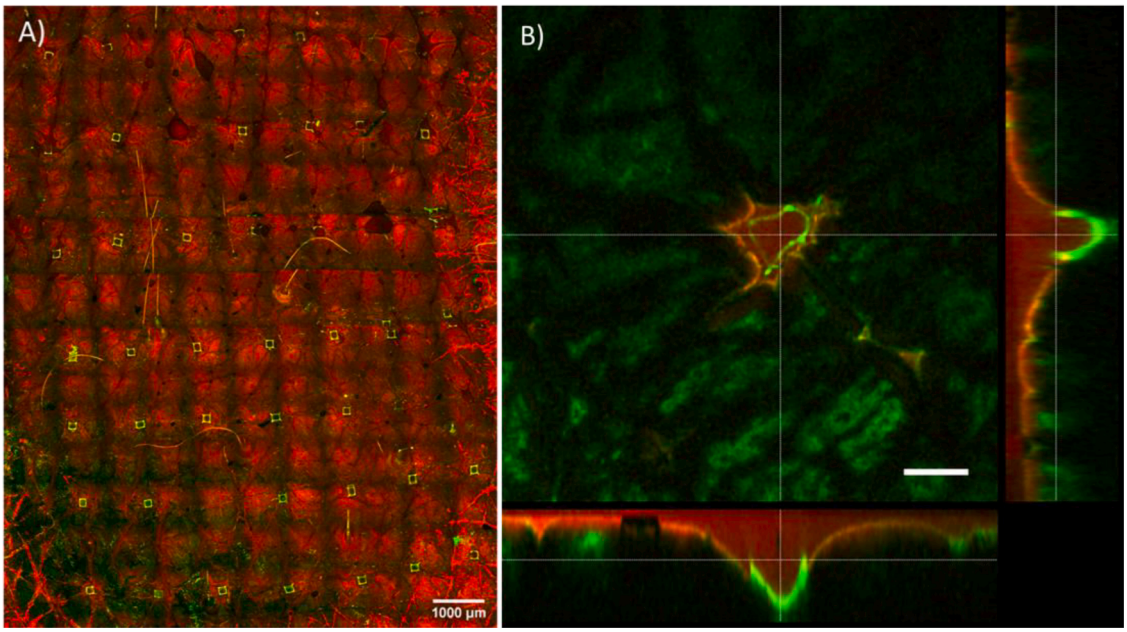

Fig. 7. Overview CARS image of needles in human dorsal skin. The red channel is the CARS signal imaged at 2850 cm-1 and the green channel is auto-fluorescence and second harmonic generation. A) surface of skin. B) The image is an optical slice taken about 100 µm under the skin surface showing the top of the needle. The panels on the bottom and right side of the image are XZ and YZ slices through the sample. Structures of collagen and live cells can be seen in the green channel clearly showing that the needle has penetrated the epidermis. In fact, the needle tip is more than 200 µm below the skin surface. The scale bar is 200 µm.

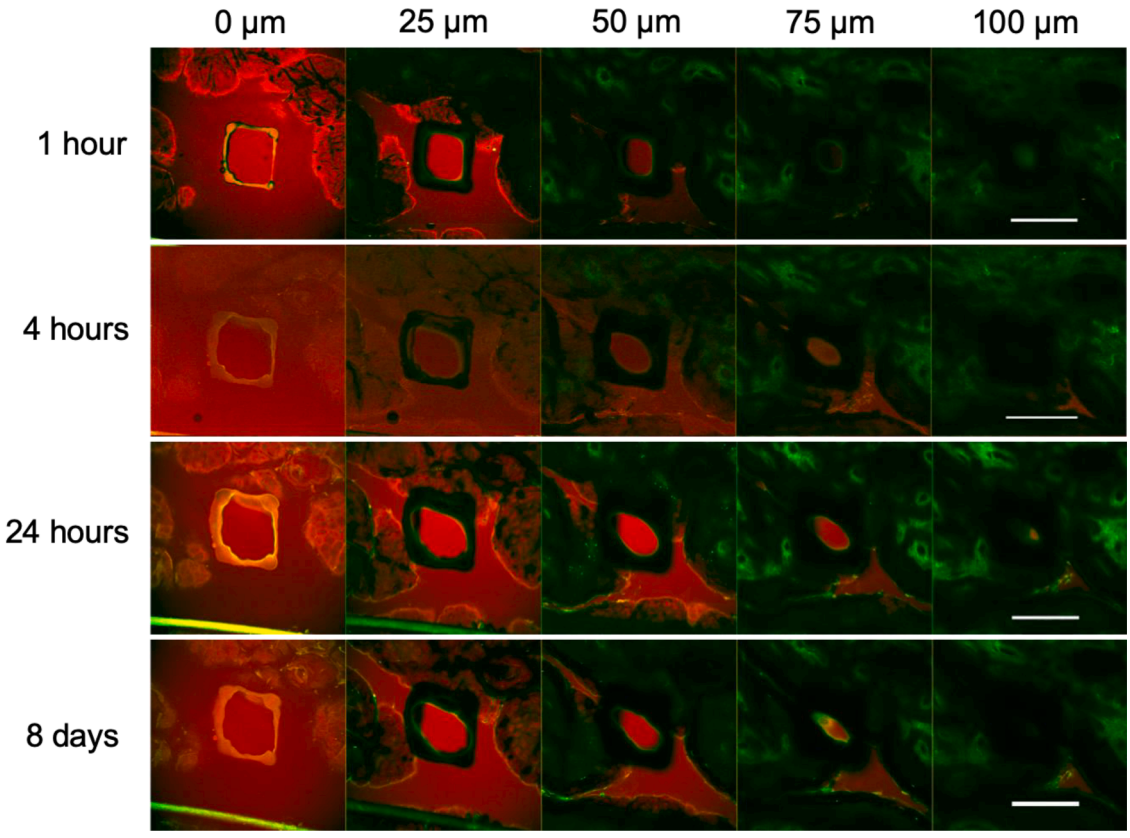

Fig. 8. CARS image of an active needle in human abdominal skin over time. The image is a montage beginning at the top of the needle moving 25 µm deeper into the skin per image. Samples were kept at 28–32C. The red channel is the CARS signal imaged at 1750 cm-1. The green channel is the autofluorescence and second harmonic generation. Scale bar is 200 µm.

tip

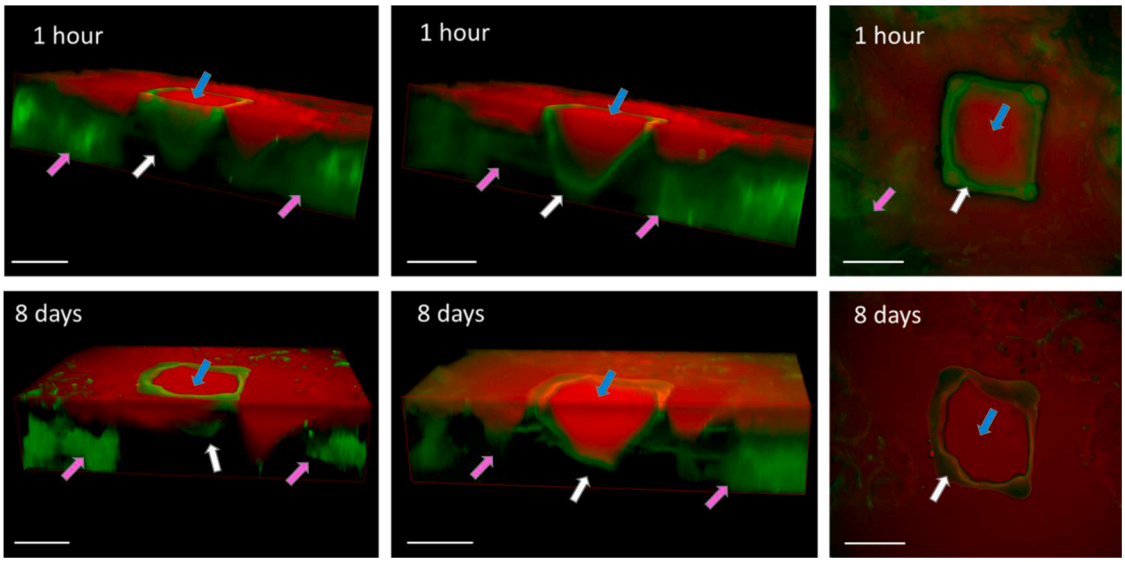

Fig. 9. 3D rendering of CARS images of an active needle in human dorsal skin after 1 hour and 8 days. The red channel is the CARS signal imaged at 1750 cm^{-1}. The green channel is auto fluorescence and second harmonic generation. White arrows show the needle tip, pink arrows show the skin tissue blue arrows show the base material. Scale bar is 100 μm.

release is highest at day 1 with a decrease on day 4 and again an increase on day 6. FKBP5 and B-17-P metabolite show a continuous increase in release throughout the duration of the experiment for both patch and gel.

In the *in vivo* studies, a different trend is observed. In both CD14 and FKBP5 the daily applied gel appears to have a larger effect on the release compared to the patch, but for B-17-P metabolite the patch reaches the same effect on day 2 as the gel on day 4.

4. Discussion

Effective cutaneous drug delivery remains challenging. The anatomical and physiological barriers of the skin lead to low bioavailability of drugs and limit the number of feasible drug choices (Alkilani et al., 2015; Sabri et al., 2019). In the work presented here dissolvable MNs with modified release of calcipotriol (Calci) and betamethasone-17–21-dipropionate (BDP) were presented. They were shown to penetrate the SC into the dermal compartment and provide modified bioavailability of the API/drugs in *ex vivo* and *in vivo* experiments.

Both the CARS images and CT scans of the microneedles applied to the skin clearly show that the patches can be used as a drug delivery system as they penetrate the SC and insert into a depth of up to 250 μm without breaking or being completely deformed to flat needles. The time laps CARS data showed that the MNs stay in the skin for over 8 days although their morphology slowly changes. This is of course a prerequisite to act as a depot for a drug delivery system and shows the promise of the microneedles for this application (Vora et al., 2021).

The CARS images showed that the remains of the fast-dissolving drug-free backing layer of the needles penetrates further into the needle tip within the first 24 h. This is thought to be due to the slow diffusion of material, from the slowly dissolving drug containing tip, into the skin creating more space for the PVP base material (see Figs. 8 and 9). This PVP material is not expected to change the delivery from the tip of the needle as the drug will mainly partition to the skin, due to the sink conditions the tissue provides. After the initial 24 h the needle morphology remained more stable. This complements the results from the *in vitro* delivery studies which showed an initial fast release followed by a more prolonged delivery. However, as the active drug could not be separated from the signal from the skin with CARS the diffusion of the drug in the skin was not directly visible. This is due to the fact that the drugs do not show any Raman signal in the Raman free signal space of skin.

The *ex vivo* and *in vitro* release experiments demonstrate that the application of the MNs stimulates an intradermal cellular response (increased CD14 and FKBP5 gene expression) as well as showing the presence of drug metabolites in the samples over an extended time period. From Fig. 9 the largest effect of the MNs relative to the time after application is seen at 1 day after application. This is in full accordance with the *in vitro* release data showing an immediate burst release of 40% of the drug dose. However, it is not yet fully understood how the *in vitro* release data directly translate into the *in vivo* settings with a less polar and water rich environment. The release *in vivo* is very likely slower which also fits with the *ex vivo* data where the one times treatment with the MNs is almost on par with the once daily treatment with the Daivobet gel®. These results reveal that the MNs indeed function as a modified -release drug delivery system with an effect comparable with the once daily application of the gel-based comparator.

However, in the *in vivo* release experiments the effect observed was different than in the *ex vivo* experiments. *In vivo*, it appeared as though the MNs had a smaller effect on the induction of CD14 and FKBP5 gene expression than the daily application of the Daivobet gel. This could be due to lateral skin motions when the pigs are moving around in the stable or rubbing against the wall in the box, resulting on outward directed forces causing the MN to fall out of the skin before complete release. Another explanation may be related to the MNs primarily releasing the drug in the vascularized dermal compartment potentially resulting in a more efficient drainage of the drug into the systemic circulation. These findings illustrate how important it is to have an effective and fast method in clinical trials to monitor whether the needles are in place in the skin or not at the different time points to ensure the correct interpretation of the PK/PD readouts. We have demonstrated in this study that CARS definitely offers the possibility to monitor a whole patch in clinical settings within a reasonable timeframe (Breunig et al., 2012). Equipping the CARS equipment with a 4 times objective, and

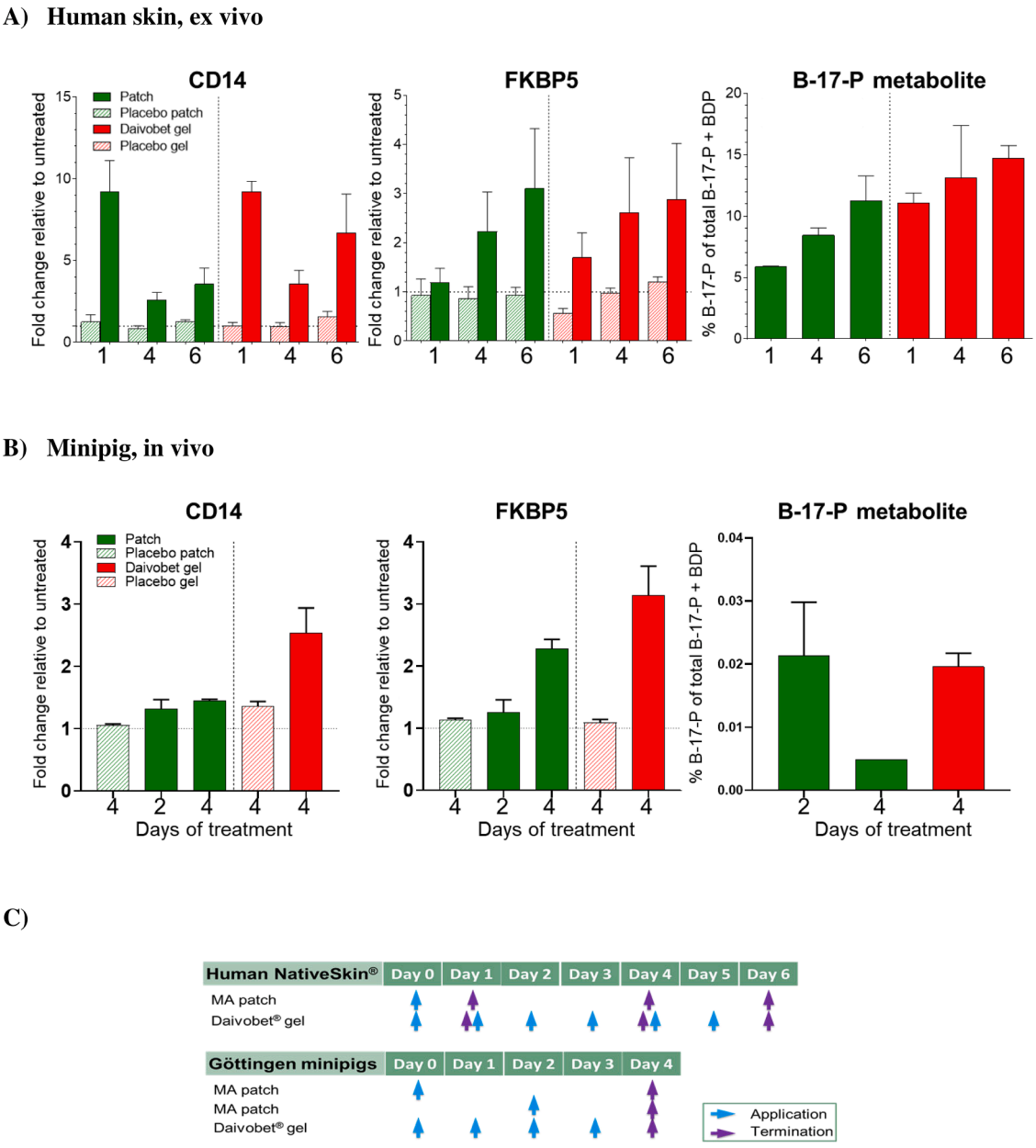

Fig. 10. Treatment responses in NativeSkin® (A) and Göttingen minipigs (B) after application of a single MNmicroneedle or daily Daivobet® Gel treatment. CD14 and FKBP5 are genes induced by calcipotriol and betamethasone-17,21-dipropionate respectively. B-17-P is the betamethasone dipropionate metabolite betamethasone-17-propionate. Outline of the application and termination schedule (C).

imaging in e.g. two different depths with an image size of 12 × 12mm^2 with a pixel resolution of 8192 × 8192 could be done within 2–4 min. The advantages of CARS and SRS compared to imaging techniques like MALDI-MSI lies their non-invasive nature makes them suitable for both lab and clinical studies and offer a spatial resolution in the submicron scale where e.g. MALDI-MSI typically is in the range between 10 and 40 μm. The disadvantage of the Raman-based techniques like CARS and SRS compared to mass spectrometry techniques is the sensitivity, where the sensitivity of CARS and SRS is in the mM range compared to the μM range of e.g. MALDI-MSI. Furthermore, the sensitivity and change of success with CARS and SRS are increased if the molecules have Raman signals in the Raman free space of the tissue, e.g. containing a nitril group or deuterated groups.

Taken together the results show that the MNs used in this work can be used for successful cutaneous drug delivery and function as modified release drug delivery systems over the period of at least 6 days. This indicates that the MNs could indeed be used as a drug delivery system with the promise of better patient compliance, by lowering the number of treatment days and overall time spent on treatment. However, the effect of normal mechanical stimulation, which could be expected when the MNs are in the skin of a patient, on the stability of the array in the skin remains to be tested. This could be done *in vivo* on patients using a CARS system for patient examination and if a suitable API was used, e.g. containing a nitrile or deuterated group, the release could also be monitored.

5. Conclusion

In this study, we demonstrate that a two-component dissolvable MN patch has the ability to penetrate both human and porcine skin and act as a depot in the skin where the release of the drug is controlled by the slow biodegradable process of the polymer in the skin. The successful

use of CARS for monitoring skin penetration opens a unique possibility for correlating penetration of numbers of needles with the PK/PD data of the patch in clinical settings. Compared to other non-invasive methods like OCT, CARS offers the possibility to see a whole patch and monitor the release of the drug if the drug molecule has an absorption in the Raman free space of skin e.g. contain a nitrile group.

These findings are essential if MN patches are going to move into clinical trials for treatments of chronic skin diseases and to see if they can live up to their high potential.

Author contributions

Irina Iachina: Writing – Original Draft preparation, Investigation – CARS analysis and data collection. André H. Eriksson: Writing – Original Draft preparation, Investigation – *In vivo* and *ex vivo* release data. Malene Bertelsen: Writing – Review & Editing, Investigation – *In vivo* and *ex vivo* release data. Karsten Petersson: Funding acquisition, Supervision, Conceptualization of the Microneedles, Writing - Review and Editing. Jörgen Jansson: Writing- Review & Editing, Resources – Microneedles, Conceptualization of the Microneedles. Pernille Kemp: Project administration, Conceptualization of the Microneedles, Writing- Review & Editing. Karen M. Engell: Writing – Review & Editing, Conceptualization of the Microneedles Investigation – *In vitro* release. Jonathan R. Brewer: Writing – Original Draft preparation, Investigation – CARS analysis and data collection. Kim T. Nielsen: Writing – Original Draft preparation, Investigation – CARS and CT analysis and data collection.

Declaration of Competing Interest

André H. Eriksson, Malene Bertelsen, Karsten Petersson, Jörgen Jansson, Pernille Kemp, Karen M. Engell and Kim T. Nielsen are or were LEO Pharma employees when the study was conducted. Irina Iachina and Jonathan R. Brewer have received funding from LEO Pharma for the CARS part of this study.

Data availability

Data will be made available on request.

Acknowledgments

We would like to thank: LTS Lohmann Therapie-Systeme AG, Andernach, Germany, for the preparation of the MN patches. Hanne Rosendal and Dina Wennike for technical assistance with ex vivo skin studies and qPCR. Morten Funch Carlsen for assistance with quantification of steroid and steroid metabolite. Channe Ogbozor Espenhain for assistance with quantification of steroid. Maj-Britt Schubert for assistance with the CT scans and insertions of array in the skin for the CARS studies.

CARS image acquisition was performed at the Danish Molecular Biomedical Imaging Center (DaMBIC, University of Southern Denmark), supported by the Novo Nordisk Foundation (NNF) (grant agreement number NNF18SA0032928).

Supplementary materials

Supplementary material associated with this article can be found, in the online version, at doi:10.1016/j.ejps.2023.106371.

References

Alkilani, A.Z., McCrudden, M.T., Donnelly, R.F., 2015. Transdermal drug delivery: innovative pharmaceutical developments based on disruption of the barrier properties of the stratum corneum. Pharmaceutics 7, 438–470.

Bal, S.M., Caussin, J., Pavel, S., Bouwstra, J.A., 2008. In vivo assessment of safety of microneedle arrays in human skin. Eur. J. Pharm. Sci. 35, 193–202.

Baumann, K.Y., Church, M.K., Clough, G.F., Quist, S.R., Schmelz, M., Skov, P.S., Anderson, C.D., Tannert, L.K., Gimenez-Arnau, A.M., Frischbutter, S., Scheffel, J., Maurer, M., 2019. Skin microdialysis: methods, applications and future opportunities-an EAACI position paper. Clin. Transl. Allergy 9, 24.

Bodenlenz, M., Dragatin, C., Liebenberger, L., Tschapeller, B., Boulgaropoulos, B., Augustin, T., Raml, R., Gatschelhofer, C., Wagner, N., Benkali, K., Rony, F., Pieber, T., Sinner, F., 2016. Kinetics of clobetasol-17-propionate in psoriatic lesional and non-lesional skin assessed by dermal open flow microperfusion with time and space resolution. Pharm. Res. 33, 2229–2238.

Bonnel, D., Legouffe, R., Eriksson, A.H., Mortensen, R.W., Pamelard, F., Stauber, J., Nielsen, K.T., 2018. MALDI imaging facilitates new topical drug development process by determining quantitative skin distribution profiles. Anal. Bioanal. Chem. 410, 2815–2828.

Breunig, H., Weinigel, M., Darvin, M., Lademann, J., König, K., 2012. Clinical Multiphoton and CARS Microscopy. SPIE.

Cevc, G., 2004. Lipid vesicles and other colloids as drug carriers on the skin. Adv. Drug Deliv. Rev. 56, 675–711.

Cormier, M., Johnson, B., Ameri, M., Nyam, K., Libiran, L., Zhang, D.D., Daddona, P., 2004. Transdermal delivery of desmopressin using a coated microneedle array patch system. J. Control Release 97, 503–511.

Denk, W., Strickler, J.H., Webb, W.W., 1990. Two-photon laser scanning fluorescence microscopy. Science 248, 73–76.

Donnelly, R.F., Morrow, D.I., McCrudden, M.T., Alkilani, A.Z., Vicente-Perez, E.M., O'Mahony, C., Gonzalez-Vazquez, P., McCarron, P.A., Woolfson, A.D., 2014. Hydrogel-forming and dissolving microneedles for enhanced delivery of photosensitizers and precursors. Photochem. Photobiol. 90, 641–647.

Donnelly, R.F.G.M.J., Morrow, D.I.J., Migalska, K., Raghu Raj Singh, T., Majithiya, R., Woolfson, A.D., 2010. Optical coherence tomography is a valuable tool in the study of the effects of microneedle geometry on skin penetration characteristics and in-skin dissolution. J. Control. Release 147, 8.

Doty, A.C., Weinstein, D.G., Hirota, K., Olsen, K.F., Ackermann, R., Wang, Y., Choi, S., Schwendeman, S.P., 2017. Mechanisms of in vivo release of triamcinolone acetonide from PLGA microspheres. J. Control. Release 256, 19–25.

El Gammal, S., El Gammal, C., Kaspar, K., Pieck, C., Altmeyer, P., Vogt, M., Ermert, H., 1999. Sonography of the skin at 100MHz enables in vivo visualization of stratum corneum and viable epidermis in palmar skin and psoriatic plaques. J. Invest. Dermatol. 113, 821–829.

Evans, C.L., Potma, E.O., Puoris'haag, M., Côté, D., Lin, C.P., Xie, X.S., 2005. Chemical imaging of tissue *in vivo*with video-rate Coherent anti-Stokes Raman scattering microscopy. Proc. Natl. Acad. Sci. 102, 16807–16812.

Evans, C.L., Xie, X.S., 2008. Coherent anti-stokes Raman scattering microscopy: chemical imaging for biology and medicine. Annu. Rev. Anal. Chem. (Palo Alto Calif) 1, 883–909.

Gomaa, Y.A., Garland, M.J., McInnes, F., El-Khordagui, L.K., Wilson, C., Donnelly, R.F., 2012. Laser-engineered dissolving microneedles for active transdermal delivery of nadroparin calcium. Eur. J. Pharm. Biopharm. 82, 299–307.

Handler, A.M., Eirefelt, S., Lambert, M., Johansson, F., Hollesen Schefe, L., Ostergaard Knudsen, N., Bodenlenz, M., Birngruber, T., Sinner, F., Huss Eriksson, A., Pommergaard Pedersen, G., Janfelt, C., Troensegaard Nielsen, K., 2021. Characterizing cutaneous drug delivery using open-flow microperfusion and mass spectrometry imaging. Mol. Pharm. 18, 3063–3072.

Haq, M.I., Smith, E., John, D.N., Kalavala, M., Edwards, C., Anstey, A., Morrissey, A., Birchall, J.C., 2009. Clinical administration of microneedles: skin puncture, pain and sensation. Biomed. Microdevices 11, 35–47.

Herwadkar, A., Sachdeva, V., Taylor, L.F., Silver, H., Banga, A.K., 2012. Low frequency sonophoresis mediated transdermal and intradermal delivery of ketoprofen. Int J Pharm 423 (2), 289–296. https://doi.org/10.1016/j.ijpharm.2011.11.041.

Ito, Y., Hirono, M., Fukushima, K., Sugioka, N., Takada, K., 2012. Two-layered dissolving microneedles formulated with intermediate-acting insulin. Int. J. Pharm. 436, 387–393.

Jakka, D., Matadh, A.V., Shankar, V.K., Shivakumar, H.N., Narasimha Murthy, S., 2022. Polymer coated polymeric (PCP) microneedles for controlled delivery of drugs (dermal and intravitreal). J. Pharm. Sci.

Kaushik, S., Hord, A.H., Denson, D.D., McAllister, D.V., Smitra, S., Allen, M.G., Prausnitz, M.R., 2001. Lack of pain associated with microfabricated microneedles. Anesth. Analg. 92, 502–504.

Khattak, S.U., Sheikh, D., Ahmad, I., Usmanghani, K., 2012. Kinetics of thermal degradation of betamethasone valerate and betamethasone dipropionate in different media. Indian J. Pharm. Sci. 74, 133–140.

Lind, M., Nielsen, K.T., Schefe, L.H., Norremark, K., Eriksson, A.H., Norsgaard, H., Pedersen, B.T., Petersson, K., 2016. Supersaturation of Calcipotriene and betamethasone dipropionate in a novel aerosol foam formulation for topical treatment of psoriasis provides enhanced bioavailability of the active ingredients. Dermatol. Ther. 6, 413–425 (Heidelb).

Liu, S., Jin, M.N., Quan, Y.S., Kamiyama, F., Katsumi, H., Sakane, T., Yamamoto, A., 2012. The development and characteristics of novel microneedle arrays fabricated from hyaluronic acid, and their application in the transdermal delivery of insulin. J. Control. Release 161, 933–941.

Loizidou, E.Z., Inoue, N.T., Ashton-Barnett, J., Barrow, D.A., Allender, C.J., 2016. Evaluation of geometrical effects of microneedles on skin penetration by CT scan and finite element analysis. Eur. J. Pharm. Biopharm. 107, 1–6.

Matsuo, K., Hirobe, S., Yokota, Y., Ayabe, Y., Seto, M., Quan, Y.S., Kamiyama, F., Tougan, T., Horii, T., Mukai, Y., Okada, N., Nakagawa, S., 2012a. Transcutaneous immunization using a dissolving microneedle array protects against tetanus, diphtheria, malaria, and influenza. J. Control. Release 160, 495–501.

Matsuo, K., Yokota, Y., Zhai, Y., Quan, Y.S., Kamiyama, F., Mukai, Y., Okada, N., Nakagawa, S., 2012b. A low-invasive and effective transcutaneous immunization system using a novel dissolving microneedle array for soluble and particulate antigens. J. Control. Release 161, 10–17.

Naito, S., Ito, Y., Kiyohara, T., Kataoka, M., Ochiai, M., Takada, K., 2012. Antigen-loaded dissolving microneedle array as a novel tool for percutaneous vaccination. Vaccine 30, 1191–1197.

Nguyen, J., Lewis, H., Queja, A., Diep, A.N., Hochart, G., Ameri, M., 2018. Pharmacokinetics and skin tolerability of intracutaneous zolmitriptan delivery in swine using adhesive dermally applied microarray. J. Pharm. Sci. 107, 2192–2197.

Norsgaard, H., Kurdykowski, S., Descargues, P., Gonzalez, T., Marstrand, T., Dunstl, G., Ropke, M., 2014. Calcipotriol counteracts betamethasone-induced decrease in extracellular matrix components related to skin atrophy. Arch. Dermatol. Res. 306, 719–729.

Petersson, K., Engell, K.M., Jansson, J., Nielsen, K.T., Eriksson, A.H., Moore, A., Vucen, S., O'Sullivan, C., Crean, A., 2016. Microneedle patch for delivering an active ingredient to skin, patent cooperation treaty (PCT).

Quinn, H.L., Kearney, M.C., Courtenay, A.J., McCrudden, M.T., Donnelly, R.F., 2014. The role of microneedles for drug and vaccine delivery. Expert Opin. Drug Deliv. 11, 1769–1780.

Ripolin, A., Quinn, J., Larraneta, E., Vicente-Perez, E.M., Barry, J., Donnelly, R.F., 2017. Successful application of large microneedle patches by human volunteers. Int. J. Pharm. 521, 92–101.

Sabri, A.H., Ogilvie, J., Abdulhamid, K., Shpadaruk, V., McKenna, J., Segal, J., Scurr, D. J., Marlow, M., 2019. Expanding the applications of microneedles in dermatology. Eur. J. Pharm. Biopharm. 140, 121–140.

Schauber, J., Dorschner, R.A., Coda, A.B., Buchau, A.S., Liu, P.T., Kiken, D., Helfrich, Y. R., Kang, S., Elalieh, H.Z., Steinmeyer, A., Zugel, U., Bikle, D.D., Modlin, R.L., Gallo, R.L., 2007. Injury enhances TLR2 function and antimicrobial peptide expression through a vitamin D-dependent mechanism. J. Clin. Invest. 117, 803–811.

Sevilla, L.M., Bayo, P., Latorre, V., Sanchis, A., Perez, P., 2010. Glucocorticoid receptor regulates overlapping and differential gene subsets in developing and adult skin. Mol. Endocrinol. 24, 2166–2178.

Sullivan, S.P., Koutsonanos, D.G., Del Pilar Martin, M., Lee, J.W., Zarnitsyn, V., Choi, S. O., Murthy, N., Compans, R.W., Skountzou, I., Prausnitz, M.R., 2010. Dissolving polymer microneedle patches for influenza vaccination. Nat. Med. 16, 915–920.

Sullivan, S.P., Murthy, N., Prausnitz, M.R., 2008. Minimally invasive protein delivery with rapidly dissolving polymer microneedles. Adv. Mater. 20, 933–938.

Saar, B.G., Freudiger, C.W., Reichman, J., Stanley, C.M., Holtom, G.R., Xie, X.S., 2010. Video-rate molecular imaging in vivo with stimulated Raman scattering. Science 330, 1368–1370.

Tanner, T., Marks, R., 2008. Delivering drugs by the transdermal route: review and comment. Skin Res. Technol. 14, 249–260.

Thorsted, A., Bouchene, S., Tano, E., Castegren, M., Lipcsey, M., Sjolin, J., Karlsson, M. O., Friberg, L.E., Nielsen, E.I., 2019. A non-linear mixed effect model for innate immune response: in vivo kinetics of endotoxin and its induction of the cytokines tumor necrosis factor alpha and interleukin-6. PLoS One 14, e0211981.

Vora, L.K., Moffatt, K., Tekko, I.A., Paredes, A.J., Volpe-Zanutto, F., Mishra, D., Peng, K., Raj Singh Thakur, R., Donnelly, R.F., 2021. Microneedle array systems for long-acting drug delivery. Eur. J. Pharm. Biopharm. 159, 44–76.

Wang, Thakur, R., Fan, Q., Michniak, B., et al., 2005, 2005. Transdermal iontophoresis: combination strategies to improve transdermal iontophoretic drug delivery. Eur J Pharm Biopharm 60 (2), 179–191. https://doi.org/10.1016/j.ejpb.2004.12.008.

Zumbusch, A., Holtom, G.R., Xie, X.S., 1999. Three-dimensional vibrational imaging by coherent anti-stokes raman scattering. Phys. Rev. Lett. 82, 4142–4145.